# Targeted Synthesis of Anti-Hydrolysis 2D-ZIF Laminates with Super-Hydrophobic Transport Channels via In Situ Phase Transition Strategy

*Shuang Xu, Wen-Cui Li, Chengtong Wang, Sijia Wang, He Ma, Guang-Ping Hao,\**
*and An-Hui Lu\**

The design flexibility in the crystalline structure and surface wettability make the zeolitic imidazolate frameworks (ZIFs) an excellent platform for task-specific applications. However, the key challenge lies in the precise modulation of transport channels, which still suffers from slow diffusion kinetics in nanopores and the loss of hydrophobicity during long-term operation. Here, a facile structural directing method to render conventional 3D polyhedrons to well-controlled ZIF nanoplates, and further to super-hydrophobic laminated material by an in situ phase transition strategy is reported. As exemplified in water transport devices, the integrated ZIFs laminate shows an exceptional anti-hydrolysis property and super-hydrophobic transport channels, which warrant remarkable structural stability at fully wet conditions for a time period of at least 3 months, even under acidic conditions and boiling water for 24 h. The simple transformation strategy paves the way for fabrication and regulation of coordinated structures where hydrophobic transport channels are required, and opens a new opportunity for the smart design of advanced structures for water treatment under harsh environments.

## 1. Introduction

Nanostructures featured with 2D morphology, exemplified by graphene, exfoliated MXenes, BN nanosheets, and 2D metal coordinated structures have been mostly used as building blocks in laminated materials for water transport-related applications because their interlayer nanochannels can provide more efficient molecular transferability than their 3D block counterparts.[1] During water transport, water molecules preferentially flow through hydrophobic channels with fast kinetic behavior. However, due to the high density of active edges and polar functional groups, the transport channels are rather hydrophilic.[2] The mass transfer resistance in water molecule transport would be increased due to the polarity interaction of water molecules with a hydrophilic surface, thus decreasing the transport

efficiency. The first prerequisite to enable high efficiency in water transport is to achieve a super-hydrophobic transport surface and channel.[3,4] Although various hydrophobic functionalization strategies were explored, it is notoriously difficult to achieve a long-lasting super-hydrophobicity under harsh wet environments.

Zeolitic imidazolate frameworks (e.g., ZIF-8) are potentially promising candidates because of their highly designable crystalline structure and relatively hydrophobic and stable feature.[5] Under the stablished synthesis procedure, the morphology of resultant ZIF-8 is 3D polyhedron,[6] which hinders the laminating processes that normally require 2D building blocks. In principle, control of crystal orientation by interfering with intrinsic coordination mode to overcome the energy barrier can achieve 2D coordinated structure. However, it is difficult to form a 2D structure for ZIF-8 because the high symmetrical tetrahedral unit of $Zn(Hmim)_4$ preferentially grows into a 3D rhombic dodecahedral or cubic shape to minimize the surface energy.[7] Moreover, the available research, including our previous studies showed that the template method could be used for the synthesis of highly cross-linked amorphous polymer nanoplates.[8] However, it still remains unsuccessful for the synthesis of 2D ZIF structure, as the coordination interaction between ligand and metal node is stronger than the interaction based on hydrogen bond between template and ligand.[9] Additionally, the coordination between the ligand and metal node is rather delicate, which is distinct to the amorphous polymer layers on the basis of a covalent bond. Thus, the controllable synthesis of 2D ZIF structure remains a huge challenge owing to the lack of an effective strategy.

In practical application, most of the available coordinated structures showed instability and decomposition for water transport due to their severe hydrolysis and collapse of the coordinated framework after long cycles in humid environments, particularly under acidic or heating conditions.[10,11] To this end, various post-functionalization or in situ modifications of the metal nodes or ligands with hydrophobic groups have been exploited.[12] Although the moisture stability of these structures indeed improved to a large extent, the hydrolysis under acidic aqueous conditions is still severe.[13] Thus, a reliable strategy to fabricate 2D ZIF-8 with a durable anti-hydrolysis is highly challenging and unsolved for coordinated structures.

S. Xu, W.-C. Li, C. T. Wang, S. J. Wang, H. Ma, G.-P. Hao, A.-H. Lu
State Key Laboratory of Fine Chemicals
Liaoning Key Laboratory for Catalytic Conversion of Carbon Resources
and School of Chemical Engineering
Dalian University of Technology
Dalian 116024, China
E-mail: guangpinghao@dlut.edu.cn; anhuilu@dlut.edu.cn

Herein, we report a facile structural directing method for the synthesis of ZIF-8 material with controllable 2D morphology and highly remarkable super-hydrophobicity, in which the hydrophobic promotor, stearic acid featured with plate-like morphology simultaneously served as structure-directing agent, and sodium dodecyl benzene sulfonate as bridging agent. Meanwhile, the stearic acid is chemically trapped in 2D-ZIF-8 units and interlocked in the interlayers to contribute the super-hydrophobicity. Upon phase transition, a ZIF laminated material with remarkably hydrophobic transport channels and anti-hydrolysis characteristic is fabricated. Exemplified for water vapor transport under a temperature gradient, the obtained material displayed a long-term stability at fully wet conditions, e.g., for a time length of at least 3 months; and surprisingly, the crystal structure was well-remained even at the acidic aqueous solution and boiling water for 24 h. In excellent accordance, the ZIF-laminated material demonstrated two times higher permeation flux than that of the pure phase ZIFs membranes and is even comparable to the reported inorganic materials. The proposed phase transition strategy might serve as a general method to advance the synthesis methodology where hydrophobic transport channels are required.

## 2. Results and Discussion

The 2D ZIF-8 (denoting 2D-ZIF-8) was prepared in the solution phase in the presence of the structure-directing agent stearic acid (SA) and bridging agent sodium dodecyl benzene sulfonate (SDBS; **Figure 1**a), and the morphology evolution was recorded by the time-dependent SEM images (Figure S1, Supporting Information). In process (I), the SDBS molecules would first adsorb to the SA micelles, and cross-linked platelike structures were formed (Figure S1a, Supporting Information); in process (II), the $Zn^{2+}$ ions were grafted to the micelles through ions exchange and $Zn\cdots O$ coordination. Then, in process (III), Hmim was introduced, and the $O\cdots Zn–Hmim$ complexes were formed through complexation of $Zn^{2+}$ with Hmim linkers, and nanoplate rudiment was generated (Figure S1b,c, Supporting Information); finally, the ZIF-8 in nanoplate form was achieved with the help of a structure-directing agent (Figure S1d, Supporting Information). To further disclose the growth process, we monitored the changes of surface charge by measuring the Zeta potential. Initially, the SA micelles showed a negative charge with a Zeta potential of −33 mV (Figure S2a, Supporting Information). After introducing the SDBS, $Zn(NO_3)_2$, and Hmim aqueous solution, in turn, the Zeta potential of the solution was
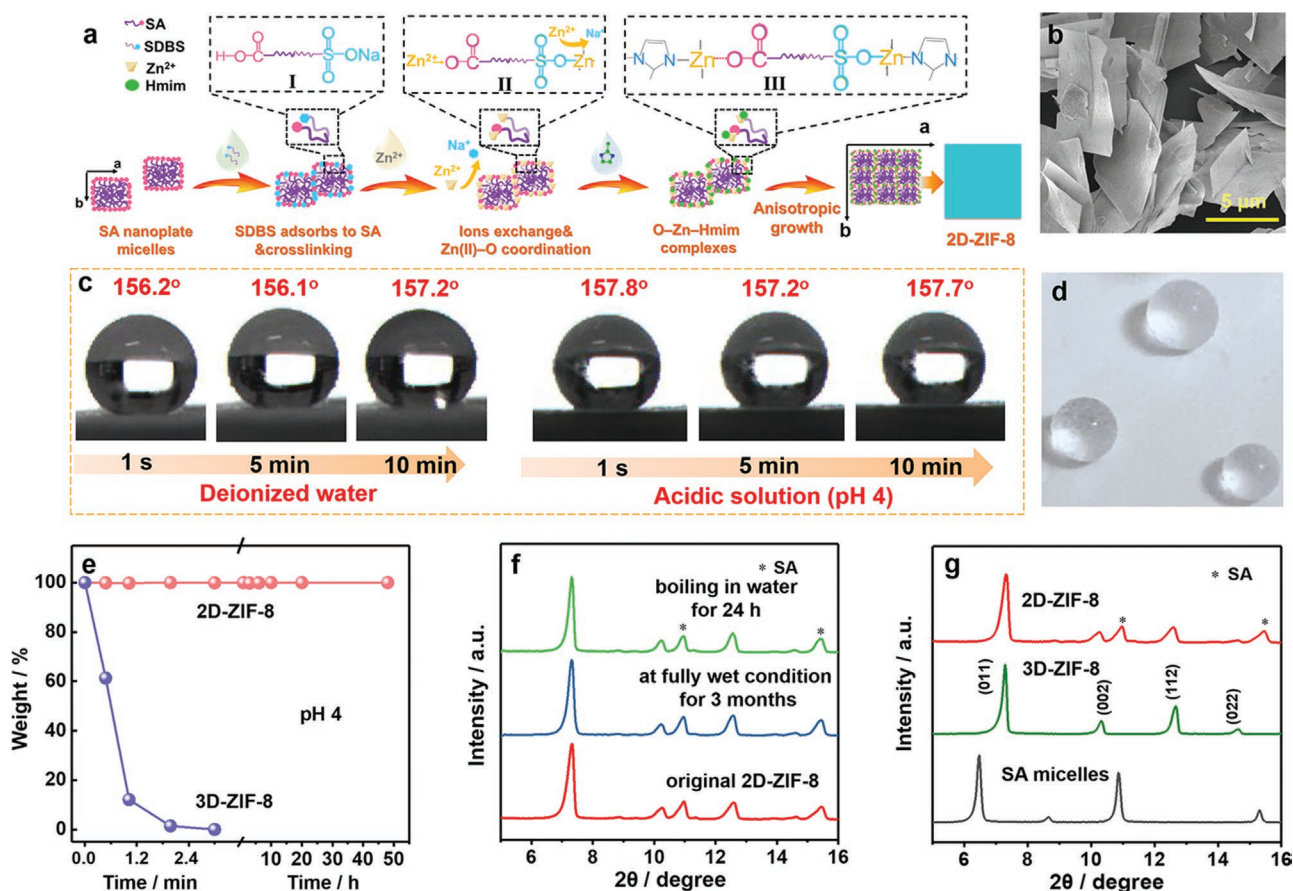


**Figure 1.** Synthesis and characterizations of 2D-ZIF-8. a) Schematic of the synthesis strategy for 2D-ZIF-8. b) SEM image of 2D-ZIF-8. c) Snapshots of contact angles of DI water and acidic aqueous solution (pH 4) on the 2D-ZIF-8 pellet at 25 °C for 10 min. d) Photograph of water droplets on the surface of 2D-ZIF-8 pellet for 10 min. e) Time-resolved degradation of the 2D-ZIF-8 and conventional 3D-ZIF-8 in acidic aqueous solution (pH 4) at 25 °C. f,g) XRD patterns.

increased to −6 mV (Figure S2b–d, Supporting Information) due to the accumulation of positive charges of $Na^+$ and $Zn^{2+}$ ions around the SA. This result evidenced the growth of ZIF seeds around the SA. Then, the 2D-ZIF-8 product was separated from the synthesis solution with a constant Zeta potential of −12 mV (Figure S2e, Supporting Information), and the quadrilateral nanoplates were obtained with a lateral dimension of around 9 μm × 9 μm (Figure 1b). The thickness of 2D-ZIF-8 was determined to be 105 ± 12.9 nm by atomic force microscopy (AFM) (Figure S3, Supporting Information).

Notably, the hydrophobic promotors, SA molecules were locked in the structure of the 2D-ZIF-8 unit during the coordination process, which could generate low surface energy due to its weak polarity and thus enable the permanent hydrophobicity of ZIF nanoplates.[10d] Such 2D-ZIF-8 displayed a constant water contact angle of around 158° even after contacting water and acidic solution for 10 min (Figure 1c,d, Figure S4, Supporting Information), indicating its superhydrophobicity. Furthermore, the 2D-ZIF-8 showed remarkable stability that it can bear the acidic and alkaline solution for more than 24 h (Figure S5a, Supporting Information); while its 3D counterpart degraded very fast, i.e., in 3 min at 25 °C (Figure 1e).

Meanwhile, the 2D-ZIF-8 exhibited exceptional anti-hydrolysis property at the fully wet conditions for at least 3 months, and the crystal structure remained well after boiling in water for >24 h (Figure 1f, Figure S5b in Supporting Information). These results strongly confirmed the stability, which is ascribed to the all-around SA cover and thus prevents the framework of 2D-ZIF-8 from wetting by the polar molecules even under harsh wet conditions. To verify this speculation, the locking state and the dispersion of SA in 2D-ZIF-8 were analyzed by the XRD technique (Figure 1g) and EDX mapping (Figure S6, Supporting Information). Besides the featured (011) and (112) diffraction peaks for 3D-ZIF-8, two visible peaks located at $2\theta$ of 10.9° and 15.4° appeared, which could be ascribed to the (00*l*) plane of the layered SA phase.[14] While the diffraction peaks at

6.4° and 8.7° for SA have not appeared in 2D-ZIF-8, probably because the SA crystallization direction is selective in the presence of the competitive coordination between SA molecules and the Zn(II) cations.[15] EDX mapping analysis showed that the main elements including C, N, O, and Zn in 2D-ZIF-8 were uniformly distributed, evidencing the well-dispersed SA domains.

The IR spectra were conducted to identify the functional groups of 2D-ZIF-8 (**Figure 2**a). The bands at 750, 1140, and 1575 cm$^{-1}$ have arisen from the N–H stretching, C–N vibration, and C=N stretching that are typical signals for ZIF-8.[16] Compared with the spectrum of SA micelles, the C=O signal in 2D-ZIF-8 shifted to low wavenumber (Figure 2a). This result was mainly attributed to the formation of the Zn···O=C structure.[15a,17] To validate this conclusion, we analyzed the surface binding features via the XPS technique. Compared with the spectra of 3D-ZIF-8, a new peak C=O at 288.5 eV[18] was observed in C 1s of 2D-ZIF-8 (Figure 2b), and the signals of O=C (531.4 eV), Zn···O=C (532.2 eV), and O···Zn (533.3 eV)[17a] were detected in O 1s spectra of 2D-ZIF-8 (Figure 2c). Accordingly, the Zn 2p spectrum of 2D-ZIF-8 shifted to high binding energy by 0.5 eV (Figure 2d) due to the coordination of O···Zn.[19] These results confirmed the existence of Zn···O=C in the 2D-ZIF-8.

After that, we employed the gas adsorption technique to identify the possible pore size and pore occupying information.[20] However, for $N_2$ and $CO_2$ adsorption, the isotherms showed a linear tendency (Figure S7, Supporting Information), suggesting the pore size is smaller than that of $N_2$ and $CO_2$,[9,21] while the He adsorption isotherm exhibited Type I sorption behavior that is indicative of porosity (Figure 2e).[22] These results confirmed that the pore size distribution of 2D-ZIF-8 should be located between 2.6 and 3.3 Å. Interestingly, the nanopores with larger pore size can be further recovered through a simple thermal treatment, which was characterized by $N_2$ adsorption (Figure 2f). It can be speculated that the mobile SA would penetrate the frameworks and expand the
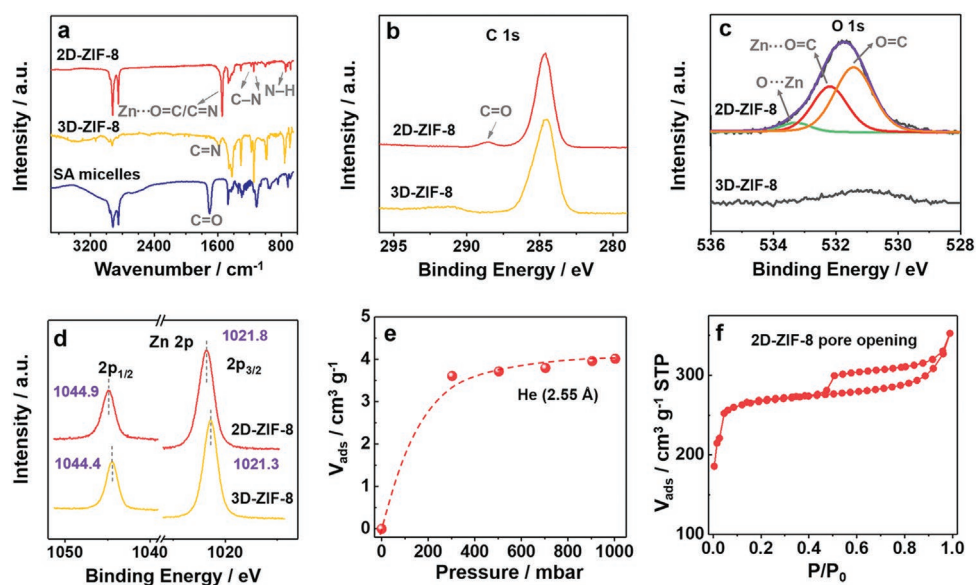


**Figure 2.** Structural characterizations of 2D-ZIF-8. a) IR spectra. b–d) C 1s, O 1s, and Zn 2p spectra. e) He adsorption isotherm at 298 K and 0–1000 mbar. f) $N_2$ adsorption–desorption isotherms at 77 K.
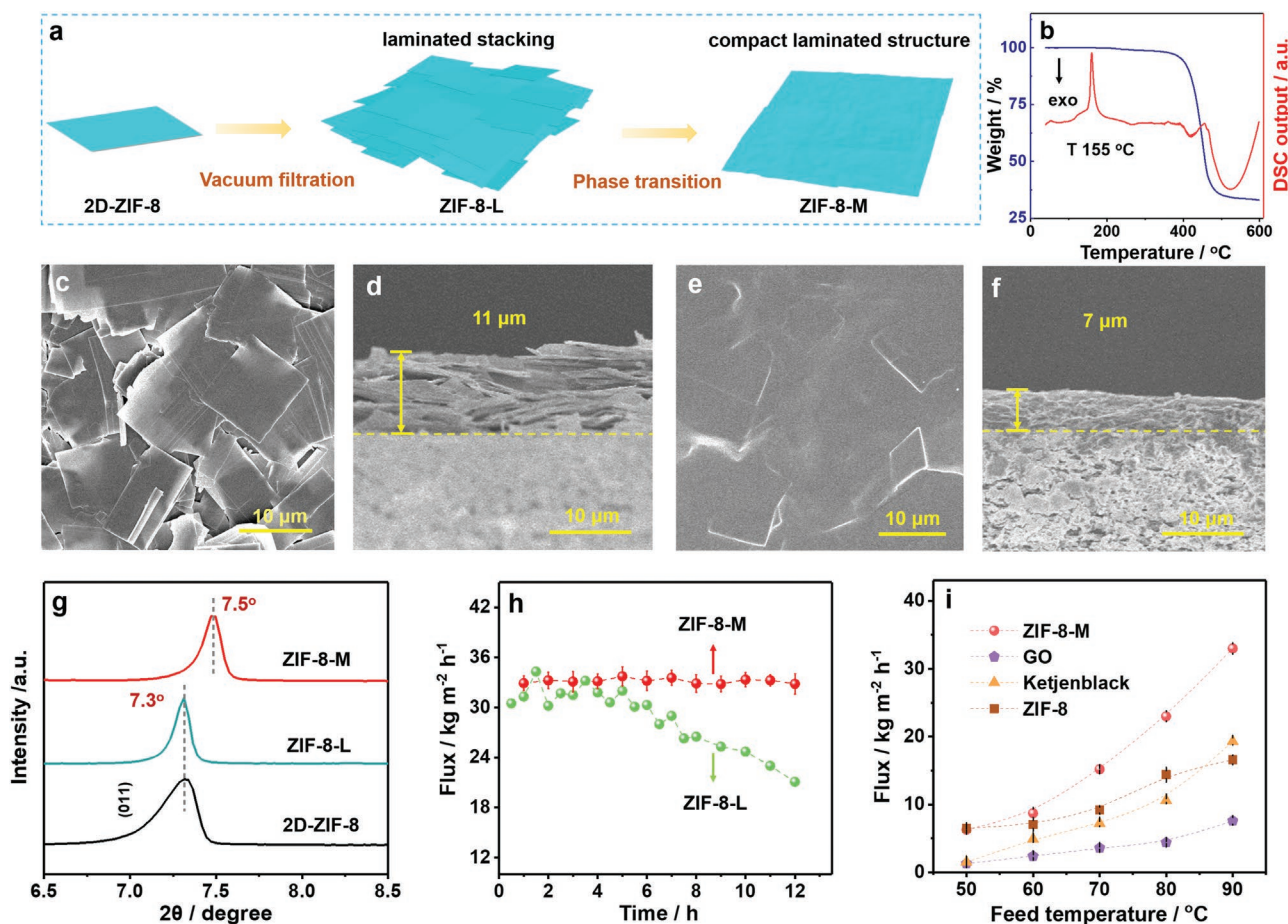
**Figure 3.** Structural characterizations of ZIF-8-L and ZIF-8-M. a) Sketch of the synthesis strategy toward the ZIF-8-M. b) The TG and DSC curves measured under argon with a heating rate of 10 °C min⁻¹. c–f) SEM images of top and cross-sectional view: c,d) ZIF-8-L, e,f) ZIF-8-M. g) XRD patterns of ZIF-8-M and ZIF-8-L. h) Desalination performances of ZIF-8-M and ZIF-8-L at feed temperature of 90 °C for 12 h. i) The relationship between water flux and feed temperature (50–90 °C) on ZIF-8-M and the benchmark materials measured on our apparatus for 12 h. Note: the water vapor outlet temperature of all tests is 25 °C. Error bars in (h) and (i) are standard deviations from at least three measurements.

interlayer/intralayer distance, and thus generate larger pores. Notably, the 2D morphology was well maintained after thermal treatment (Figure S8, Supporting Information). The calculated specific surface area was determined to be 1087 m² g⁻¹, which is close to the typical 3D-ZIF-8.

As discussed above, the hydrophobicity promotors were distributed on molecular level and chemically trapped in 2D-ZIF-8 unit, and the pore size is suitable for the transport of water vapor molecules (2.64 Å). Following, we assembled the 2D-ZIF-8 into laminated structure (ZIF-8-L) via vacuum filtration (Figure S9, Supporting Information), and investigated the water transport behavior. Upon a facile in situ phase transition process of SA promotors, ZIF-8-L transformed into the compact and integrated ZIF-8 laminate (ZIF-8-M; **Figure 3**a). Because of the solid–liquid transition under thermal treatment, the high mobility of the liquid SA promotors readily covered the defect sites of the ZIF-8-L and filled the interstitial voids, warranting a homogeneous coating of the hydrophobic layer all around the ZIF-8-L, and further ensures the formation of the ZIF-8-M with permanent hydrophobicity and integrity. The phase transition process was revealed by thermogravimetry (TG) and differential

scanning calorimetry (DSC) (Figure 3b; Figure S10, Supporting Information). The evident endothermic peak at about 155 °C was observed but no weight loss was detected, evidencing the phase transition of the trapped SA.

We then monitored the microstructure evolution of ZIF-8-L during the phase transition process toward ZIF-8-M. Before the phase transition, ZIF-8-L comprise loosely packed nanoplates (Figure 3c,d), then it became highly compact with the interstitial voids sealed after in situ phase transition (Figure 3e,f). In spite of the presence of individually scattered nanoplates on the surface of ZIF-8-M (Figure S11a, Supporting Information), the whole structure inside remains highly integrated and compact as seen from the top view (100 μm × 100 μm; Figure S11b,c, Supporting Information) and cross-sectional view (Figure S11d,e, Supporting Information). The thickness reduction from 11 μm (ZIF-8-L) to 7 μm (ZIF-8-M) before and after phase transition also evidenced the more compact feature of ZIF-8-M. Meanwhile, the crystalline structures of the ZIF-8-L and ZIF-8-M were investigated by the XRD technique (Figure 3g). The ZIF-8-L showed a highly preferred orientation as evidenced by the (011) peak at 7.3°,

which shifted to 7.5° in ZIF-8-M after phase transition, again suggesting the formation of a more compact structure with narrow interlayer spacing.

In the following, the prototype desalination device based on the ZIF-8-M was fabricated, and the water transport performance was evaluated, in which the freshwater was collected through condensation at the outlet. Notably, the ZIF-8-M exhibited a stable average permeation flux (33 kg m$^{-2}$ h$^{-1}$) and almost no degradation was detected after continuously permeating for 12 h, in contrast, the pre-phase-transition counterpart ZIF-8-L started to decrease after around 6 h under identical conditions (Figure 3h). This result verified that the ZIF-8-M with sealed interlayer voids improved the stability during the water transport process. The salt rejection of ZIF-8-M was estimated as 99.9%. The high salt rejection can be attributed to the superhydrophobicity of the transport channels, which prevents membrane flooding and size blocking of hydrated ions. We also investigated the effect of the lateral dimension of 2D-ZIF-8 nanoplates on water transport performance. The 2D-ZIF-8 nanoplates with different sizes of 8 μm × 18 μm × 0.08 μm and 20 μm × 25 × 0.3 μm were fabricated by varying the molar ratio of Zn$^{2+}$: Hmim to 1:17 (Figure S12a, Supporting Information) and 1:67 (Figure S12b, Supporting Information) at the same fabrication condition, respectively. XRD patterns and water contact angle analysis confirmed that they had identical crystal structure and superhydrophobicity compared to ZIF-8-L (Figure S12c, Supporting Information). The water transport results indicated that the narrower or thicker nanoplates would result in unstable water transport performances (Figure S12d, Supporting Information) due to the less compact laminated structures.

Moreover, we tested other materials with similar porous structure, which includes graphene oxide membranes (GO), carbon black membranes (Ketjenblack), conventional ZIF-8 membranes (Figure 3i). The ZIF-8-M exhibited higher water transport performance than that of the GO and Ketjenblack membranes at test temperature of 50–90 °C. At 50 °C, ZIF-8-M and its counterpart 3D ZIF-8 both showed a similar flux of 6.3 kg m$^{-2}$ h$^{-1}$. At higher temperatures of 80 and 90 °C, the superhydrophobic ZIF-8-M outperformed the 3D ZIF-8. Notably, it is 3–16 times higher than that of reported zeolite membranes (ZMS-5: 11.5 kg m$^{-2}$ h$^{-1}$, 75 °C,[23] NaA: 1.9 kg m$^{-2}$ h$^{-1}$, 69 °C[24]) at similar conditions. Compared with coordinated structures, ZIF-8-M showed outstanding water resistance and high water transport performance at a test temperature of 60 °C (Figure S13, Supporting Information), and the flux is approximately two times higher than that of the reported pure phase ZIF-8 membrane (20.1 vs 10.8 kg m$^{-2}$ h$^{-1}$[25], 75 °C; Figure S14, Supporting Information), that is grown on the α-Al$_2$O$_3$ substrate by solvothermal reaction (**Figure 4**a; Table S1, Supporting Information).[26] The impressive desalination performance is attributed to the significant stability and anti-hydrolysis properties.

Additionally, ZIF-8-M showed stable water transport performance not only in the neutral aqueous solution but also in acidic conditions. For example, ZIF-8-M could stably work at acidic condition (pH 4) for at least 20 h and delivered a high flux of around 32.5 kg m$^{-2}$ h$^{-1}$ over the whole operation duration, which is close to the value at neutral condition (33 kg m$^{-2}$ h$^{-1}$; Figure 4b). Furthermore, we investigated the influence of feed temperatures
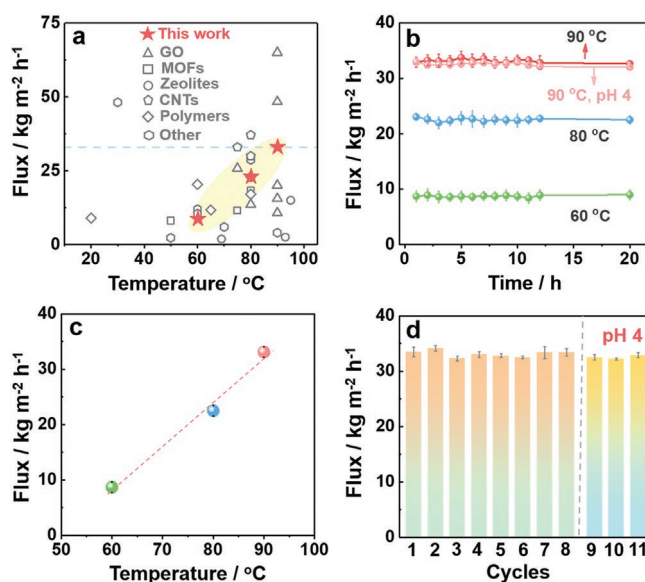


**Figure 4.** Desalination performances. a) Comparison of water flux for ZIF-8-M with the reported data. b) Permeation flux of ZIF-8-M at feed temperature of 60, 80, and 90 °C for 20 h, respectively. c) The relationship between flux and feed temperature. d) The cyclic experiments of ZIF-8-M at 90 °C in water and acidic solution (pH 4) measured for 12 h. Note: the water vapor outlet temperature of all tests is 25 °C. Error bars in (b–d) are standard deviations from at least three measurements.

on water transport. After operation at 90 °C for 20 h, the same ZIF-8-M were directly applied at 80 and 60 °C. We observed good linearity between the permeation flux and feed temperature, which indicated thermal and mechanical stability (Figure 4c). Moreover, the ZIF-8-M presented an average permeation flux of 33 kg m$^{-2}$ h$^{-1}$ after being repeatedly used for more than ten cycles at neutral and acidic conditions (Figure 4d).

## 3. Conclusion

In summary, we reported a facile solution synthesis of a novel kind of the 2D ZIF structure by collaborative structural directing method. In this synthesis, the binary molecular regulators of SA and SDBS are found effective in regulating the 2D assembly. On the one hand, the platelike SA served as structural directing agent and the SDBS as bridging agent, which together induce the growth of ZIF seeds along the horizontal direction; on the other hand, the SA served as hydrophobic molecular promotors, which were chemically trapped in the coordinated structures and interlocked in the interlayers, and thus contributed a superhydrophobic property of 2D ZIF-8. During the subsequent phase transition, the high mobility of the hydrophobic SA homogeneously covered the interlayer voids and the defect sites, and induced the formation of compact and superhydrophobic laminated ZIF-8-M. By doing so, the obtained ZIF-8-M exhibited a high-water flux, superior durability, and repeatability even in acidic aqueous solution. This fabrication strategy holds great potential for designing hydrophobic transport channels, and provides an effective method to develop diversified 2D hydrophobic nanomaterials.

## 4. Experimental Section

*Chemicals*: All chemicals were used without further purification. Zinc nitrate hexahydrate ($Zn(NO_3)_2 \cdot 6H_2O$), stearic acid (SA), and hexadecyl trimethyl ammonium bromide (CTAB) were supplied from Sinopharm Chemical Reagent Co., Ltd., 2-methylimidazole (Hmim) of 99% was purchased from the J&K Scientific Ltd. (Beijing, China), and sodium dodecylbenzenesulfonate (SDBS) was supplied from Bodi Chemical Co., Ltd. (Tianjin, China). Pluronic F127 was purchased from Sigma–Aldrich.

*Synthesis of SA Micelles*: In a typical synthesis, 0.2 g F127 was dissolved in 20 mL deionized water at 40 °C. The resultant solution was heated to 80 °C, then 0.14 g SA was added to the hot aqueous solution. By means of vigorous stirring for 6 h and subsequently incubating for 24 h under 25 °C with static conditions, a stable SA micelles solution was obtained.

*Preparation of 2D-ZIF-8*: First, 20 mL SA micelles solution was dissolved in 330 mL water at 25 °C, then 0.4 mmol SDBS was added for 15 min. After that, 30 mL 0.02 mol L$^{-1}$ $Zn(NO_3)_2$ solution was poured into the former under stirring condition for 30 min, subsequently, different concentrations of Hmim aqueous were added to the above solution with stirring 2 h and further heated to 60 °C for 17 h. The 2D-ZIF-8 nanoplates were obtained through centrifugation and water wash. The yield of 2D-ZIF-8 was ≈42% based on the amount of zinc.

*Preparation of ZIF-8-L and ZIF-8-M*: Before the fabrication of laminated structures, the precursor solution was ultrasound for 15 min. Then, the ZIF-8-L was prepared using a diluted 2D-ZIF-8 solution (0.1 mg mL$^{-1}$) through filtering on the mixed cellulose ester substrate. After that, the ZIF-8-L was dried in a vacuum oven at 25 °C for 12 h. Then the ZIF-8-L was treated at 155 °C for 10, 30, and 60 min, respectively. It can be found that the 10 min treatment resulted in an insufficient phase transition, failing to form the compact membrane; while the treatment for 60 min led to the formation of a relatively fragile membrane. While the 30 min treatment was sufficient for the phase transition, and the resultant membrane was compact and integrated. In addition, we observed that the ZIF-8-M became brittle when the heat time was long as 60 min, causing the separation of the membrane from the substrate. Therefore, 30 min was set as the optimized treatment time. The obtained material was denoted as ZIF-8-M.

*Prototype Water Vapor Transport Evaluation*: The water vapor flux across the ZIF laminated material was measured by monitoring the weight of the solution in the distillate reservoir using the digital balance, and the data were collected for each hour.[4c] During the water transport measurements, the feed temperature ranged from 50 to 90 °C that was controlled by a heater; the temperature of water vapor outlet was kept at ambient temperature (25 °C). To accelerate the collection of water distillate, we put a cold glass slide to face the water vapor (see the schematic diagram in Figure S15, Supporting Information). For each condition, at least three measurements were measured and the average value was used for data plotting. To evaluate the repeatability of the ZIF-8-M, more than ten cycles were investigated. During every operation, the ZIF-8-M was tested for 3 h and then washed with DI water for the next experiment. Before the experiments, we recorded the conductivity of standard liquid by a conductivity meter (DDS-11A, Shanghai Lei-ci Co., Ltd.), and a function between NaCl concentration in solution and conductivity was obtained.[27] Then, the conductivity of the collected distillate was measured after collecting distillate water for 20 h, and subsequently the salt rejection was calculated using the equation: $\beta = (1 - C_p/C_f) \times 100\%$, where $C_p$ and $C_f$ are the NaCl concentrations in permeate and feed solution, respectively.

*Characterization*: Scanning electron microscope (SEM) images were obtained with a Hitachi UHR FE-SEM SU8200 instrument. The BET method was used to calculate the specific surface areas ($S_{BET}$). X-ray diffraction (XRD) patterns were collected with a Panalytical X'pert Pro Super X-ray diffractometer using Cu K$_a$ radiation (40 kV, 40 mA, $\lambda$ =0.15418 nm) with a scanning angle ($2\theta$) of 5–50°. The surface charges and micelle sizes were carried out at 25–60 °C on a Malvern Zeta sizer Nano ZS90 Instrument. The FT-IR spectra were collected on a Nicolet 6700 FT-IR spectrometer. TG and DSC were conducted on an STA 449 F3 (NETZSCH) thermogravimetric analyzer under argon with a heating rate of 10 °C min$^{-1}$. X-ray photoelectron spectra (XPS) analysis was carried out with a Thermo VG ESCALAB Xl+ Microprobe instrument using Al K$_\alpha$ radiation as the X-ray source. The binding energy of the element was calibrated using a C 1s photoelectron peak at 284.6 eV. Atomic force microscopy (AFM) images were obtained with Nanowizard4XP instrument (Bruker Co.). The measurements were performed on scanning areas of 15 × 15 µm$^2$. The data were collected from at least three regions on AFM images. The wetting behavior of the material surface with water was evaluated with contact angle measurements (HARKE-SPCA, Beijing, China), and the snapshots of contact angle were captured every 30 s by a camera in the measurement system. The diameter and volume shrinkage of droplets (assumed as ideal spheres) were calculated to be 8.9% and 24.6% (Figure S4, Supporting Information). In order to consistently compare the contact angle, the sphere size was kept the same in the presented figure in the manuscript.

## Supporting Information

Supporting Information is available from the Wiley Online Library or from the author.

## Conflict of Interest

The authors declare no conflict of interest.

## Data Availability Statement

The data that support the findings of this study are available from the corresponding author upon reasonable request.

[1] a) Y. Su, E. Prestat, C. Hu, V. K. Puthiyapura, M. Neek-Amal, H. Xiao, K. Huang, V. G. Kravets, S. J. Haigh, C. Hardacre, F. M. Peeters, R. R. Nair, *Nano Lett.* **2019**, *19*, 4678; b) X. Hu, J. Zhu, *Adv. Funct. Mater.* **2020**, *30*, 1907234; c) X. Chen, S. Mohammed, G. Yang, T. Qian, Y. Chen, H. Ma, Z. Xie, X. Zhang, G. P. Simon, H. Wang, *Adv. Mater.* **2020**, *32*, 2002320; d) H. Dou, B. Jiang, M. Xu, Z. Zhang, G. Wen, F. Peng, A. Yu, Z. Bai, Y. Sun, L. Zhang, Z. Jiang, Z. Chen, *Angew. Chem., Int. Ed.* **2019**, *58*, 13969; e) H. Chen, Z. Yang, Z. Zhang, Z. Chen, M. Chi, S. Wang, J. Fu, S. Dai, *Angew. Chem., Int. Ed.* **2019**, *58*, 10626.

[2] a) B. Mi, *Science* **2014**, *343*, 740; b) L. Chen, G. Shi, J. Shen, B. Peng, B. Zhang, Y. Wang, F. Bian, J. Wang, D. Li, Z. Qian, G. Xu, G. Liu, J. Zeng, L. Zhang, Y. Yang, G. Zhou, M. Wu, W. Jin, J. Li, H. Fang, *Nature* **2017**, *550*, 380; c) Q. Yang, Y. Su, C. Chi, C. T. Cherian, K. Huang, V. G. Kravets, F. C. Wang, J. C. Zhang, A. Pratt, A. N. Grigorenko, F. Guinea, A. K. Geim, R. R. Nair, *Nat. Mater.* **2017**, *16*, 1198; d) Y. Peng, Y. Li, Y. Ban, H. Jin, W. Jiao, X. Liu, W. Yang, *Science* **2014**, *346*, 1356.

[3] a) S. Zhao, C. Jiang, J. Fan, S. Hong, P. Mei, R. Yao, Y. Liu, S. Zhang, H. Li, H. Zhang, C. Sun, Z. Guo, P. Shao, Y. Zhu, J. Zhang, L. Guo, Y. Ma, J. Zhang, X. Feng, F. Wang, H. Wu, B. Wang, *Nat. Mater.* **2021**, *20*, 1551; b) H. Lu, W. Shi, F. Zhao, W. Zhang, P. Zhang, C. Zhao, G. Yu, *Adv. Funct. Mater.* **2021**, *31*, 2101036.

[4] a) D. Ghim, X. Wu, M. Suazo, Y.-S. Jun, *Nano Energy* **2021**, *80*, 105444; b) Y. Kuang, C. Chen, S. He, E. M. Hitz, Y. Wang, W. Gan, R. Mi, L. Hu, *Adv. Mater.* **2019**, *31*, 1900498; c) W. Wang, X. Du, H. Vahabi, S. Zhao, Y. Yin, A. K. Kota, T. Tong, *Nat. Commun.* **2019**, *10*, 3220.

[5] a) M. R. S. Kebria, A. Rahimpour, G. Bakeri, R. Abedini, *Desalination* **2019**, *450*, 21; b) Y. Xiao, W. Zhang, Y. Jiao, Y. Xu, H. Lin, *J. Membr. Sci.* **2021**, *624*, 119101; c) J. Yang, Y.-B. Zhang, Q. Liu, C. A. Trickett, E. Gutiérrez-Puebla, M. Á. Monge, H. Cong, A. Aldossary, H. Deng, O. M. Yaghi, *J. Am. Chem. Soc.* **2017**, *139*, 6448; d) H. Lia, H. Liu, W. Shi, H. Zhang, R. Zhou, X. Qin, *Sep. Purif. Technol.* **2020**, *251*, 117348.

[6] a) K. Shen, L. Zhang, X. Chen, L. Liu, D. Zhang, Y. Han, J. Chen, J. Long, R. Luque, Y. Li, B. Chen, *Science* **2018**, *359*, 206; b) M. Zhao, Q. Lu, Q. Ma, H. Zhang, *Small Methods* **2017**, *1*, 1600030; c) X. Jiang, S. He, G. Han, J. Long, S. Li, C. H. Lau, S. Zhang, L. Shao, *ACS Appl. Mater. Interfaces* **2021**, *13*, 11296; d) K. Jayaramulu, J. Masa, D. M. Morales, O. Tomanec, V. Ranc, M. Petr, P. Wilde, Y.-T. Chen, R. Zboril, W. Schuhmann, R. A. Fischer, *Adv. Sci.* **2018**, *5*, 1801029; e) T. Wang, Z. Kou, S. Mu, J. Liu, D. He, I. S. Amiinu, W. Meng, K. Zhou, Z. Luo, S. Chaemchuen, F. Verpoort, *Adv. Funct. Mater.* **2018**, *28*, 1705048.

[7] a) P. Y. Moh, P. Cubillas, M. W. Anderson, M. P. Attfield, *J. Am. Chem. Soc.* **2011**, *133*, 13304; b) N. Yanai, M. Sindoro, J. Yan, S. Granick, *J. Am. Chem. Soc.* **2013**, *135*, 34; c) F. Yang, H. Mu, C. Wang, L. Xiang, K. X. Yao, L. Liu, Y. Yang, Y. Han, Y. Li, Y. Pan, *Chem. Mater.* **2018**, *30*, 3467; d) M. Malekmohammadi, S. Fatemi, M. Razavian, A. Nouralishahi, *Solid State Sci.* **2019**, *91*, 108; e) A. Sanchez-Iglesias, N. Winckelmans, T. Altantzis, S. Bals, M. Grzelczak, L. M. Liz-Marzan, *J. Am. Chem. Soc.* **2017**, *139*, 107.

[8] a) X. Xi, D. Wu, L. Han, Y. Yu, Y. Su, W. Tang, R. Liu, *ACS Nano* **2018**, *12*, 5436; b) S. Xu, W.-C. Li, C.-T. Wang, L. Tang, G.-P. Hao, A.-H. Lu, *Angew. Chem., Int. Ed.* **2021**, *60*, 6339; c) P.-F. Liu, K. Tao, G.-C. Li, M.-K. Wu, S.-R. Zhu, F.-Y. Yi, W.-N. Zhao, L. Han, *Dalton Trans.* **2016**, *45*, 12632.

[9] D. W. Kang, M. Kang, H. Kim, J. H. Choe, D. W. Kim, J. R. Park, W. R. Lee, D. Moon, C. S. Hong, *Angew. Chem., Int. Ed.* **2019**, *58*, 16152.

[10] Y. Zhan, S. He, J. Hu, S. Zhao, G. Zeng, M. Zhou, G. Zhang, A. Sengupta, *J. Hazard. Mater.* **2020**, *388*, 121752.

[11] a) C. Avci, J. Ariñez-Soriano, A. Carné-Sánchez, V. Guillerm, C. Carbonell, I. Imaz, D. Maspoch, *Angew. Chem., Int. Ed.* **2015**, *54*, 14417; b) J. B. DeCoste, G. W. Peterson, B. J. Schindler, K. L. Killops, M. A. Browe, J. J. Mahle, *J. Mater. Chem. A* **2013**, *1*, 11922;

c) S. H. Pang, C. Han, D. S. Sholl, C. W. Jones, R. P. Lively, *Chem. Mater.* **2016**, *28*, 6960; d) M.-M. Xu, Q. Chen, L.-H. Xie, J.-R. Li, *Coord. Chem. Rev.* **2020**, *421*, 213421.

[12] a) G. Huang, Q. Yang, Q. Xu, S.-H. Yu, H.-L. Jiang, *Angew. Chem., Int. Ed.* **2016**, *55*, 7379; b) C. K. Brozek, M. Dinca, *J. Am. Chem. Soc.* **2013**, *135*, 12886; c) D. Sun, Z. Li, *Chin. J. Chem.* **2017**, *35*, 135; d) L.-H. Xie, M.-M. Xu, X.-M. Liu, M.-J. Zhao, J.-R. Li, *Adv. Sci.* **2020**, *7*, 1901758; e) J. Su, N. Xu, R. Murase, Z.-M. Yang, D. M. D'Alessandro, J.-L. Zuo, J. Zhu, *Angew. Chem., Int. Ed.* **2021**, *60*, 4789.

[13] Y. Sun, Q. Sun, H. Huang, B. Aguila, Z. Niu, J. A. Perman, S. Ma, *J. Mater. Chem. A* **2017**, *5*, 18770.

[14] P. S. He, J. M. Bai, B. Xu, T. Z. Wang, *Chem. J. Chinese U.* **1989**, *3*, 284.

[15] a) K. Pielichowska, S. Głowinkowski, J. Lekki, D. Biniaś, K. Pielichowski, J. Jenczyk, *Eur. Polym. J.* **2008**, *44*, 3344; b) Y. Wang, L. Feng, J. Pang, J. Li, N. Huang, G. S. Day, L. Cheng, H. F. Drake, Y. Wang, C. Lollar, J. Qin, Z. Gu, T. Lu, S. Yuan, H.-C. Zhou, *Adv. Sci.* **2019**, *6*, 1802059.

[16] a) Q. Lai, Y. Zhao, Y. Liang, J. He, J. Chen, *Adv. Funct. Mater.* **2016**, *26*, 8334; b) E. Shi, H. Lin, Q. Wang, F. Zhang, S. Shi, T. Zhang, X. Li, H. Niu, F. Qu, *Dalton Trans.* **2017**, *46*, 554; c) M. Hayashi, D. T. Lee, M. D. de Mello, J. A. Boscoboinik, M. Tsapatsis, *Angew. Chem., Int. Ed.* **2021**, *60*, 9316.

[17] a) X. Ruan, X. Zhang, Z. Zhou, X. Jiang, Y. Dai, X. Yan, G. He, *Sep. Purif. Technol.* **2019**, *214*, 95; b) C. Serre, F. Millange, C. Thouvenot, M. Noguès, G. Marsolier, D. Louër, G. Férey, *J. Am. Chem. Soc.* **2002**, *124*, 13519.

[18] M. Oschatz, J. P. Hofmann, T. W. van Deelen, W. S. Lamme, N. A. Krans, E. J. M. Hensen, K. P. de Jong, *ChemCatChem* **2017**, *9*, 620.

[19] a) D. Pan, S. Xu, Y. Miao, N. Xu, H. Wang, X. Song, L. Gao, G. Xiao, *Catal. Sci. Technol.* **2019**, *9*, 739; b) H. Zhou, H. Xiong, R. Zhang, L. Zhang, L. Zhang, L. Li, W. Zhang, Z. Zhu, Z-A. Qiao, *Small* **2021**, *17*, 2100428; c) X. Tang, J.-Y. Zhang, B. Mei, X. Zhang, Y. Liu, J. Wang, W. Li, *Chem. Eng. J.* **2021**, *404*, 126529.

[20] a) S. Kim, T. W. Pechar, E. Marand, *Desalination* **2006**, *192*, 330; b) H. S. Cho, J. Yang, X. Gong, Y.-B. Zhang, K. Momma, B. M. Weckhuysen, H. Deng, J. K. Kang, O. M. Yaghi, O. Terasaki, *Nat. Chem.* **2019**, *11*, 562.

[21] Z. Zeng, K. Li, K. Wei, Y. Dai, L. Yan, H. Guo, X. Luo, *Chin. J. Catal.* **2017**, *38*, 498.

[22] A. C. Sudik, A. R. Millward, N. W. Ockwig, A. P. Côté, J. Kim, O. M. Yaghi, *J. Am. Chem. Soc.* **2005**, *127*, 7110.

[23] M. Drobek, C. Yacou, J. Motuzas, A. Julbe, L. Ding, J. C. D. da Costa, *J. Membr. Sci.* **2012**, *415–416*, 816.

[24] C. H. Cho, K. Y. Oh, S. K. Kim, J. G. Yeo, P. Sharma, *J. Membr. Sci.* **2011**, *371*, 226.

[25] a) Y. Mao, Q. Huang, B. Meng, K. Zhou, G. Liu, A. Gugliuzza, E. Drioli, W. Jin, *J. Membr. Sci.* **2020**, *611*, 118364; b) Y. Qian, C. Zhou, A. Huang, *Carbon* **2018**, *136*, 28; c) X. Qian, N. Li, Q. Wang, S. Ji, *Desalination* **2018**, *438*, 83; d) K. Xu, B. Feng, C. Zhou, A. Huang, *Chem. Eng. Sci.* **2016**, *146*, 159; e) B. Liang, W. Zhan, G. Qi, S. Lin, Q. Nan, Y. Liu, B. Cao, K. Pan, *J. Mater. Chem. A* **2015**, *3*, 5140.

[26] Y. Zhu, K. M. Gupta, Q. Liu, J. Jiang, J. Caro, A. Huang, *Desalination* **2016**, *385*, 75.

[27] Y. Dong, L. Ma, C. Y. Tang, F. Yang, X. Quan, D. Jassby, M. J. Zaworotko, M. D. Guiver, *Nano Lett.* **2018**, *18*, 5514.